Eur. J. Mineral.
2007, **19**, 533–546
Published online August 2007

Rb-Cs-rich rasvumite and sector-zoned "loparite-(Ce)" from Mont Saint-Hilaire (Québec, Canada) and their petrologic significance

ANTON R. CHAKHMOURADIAN[1], NORMAN M. HALDEN[1], ROGER H. MITCHELL[2] and LÁSZLÓ HORVÁTH[3]

[1] Department of Geological Sciences, University of Manitoba, Winnipeg, Manitoba, R3T 2N2, Canada
*Corresponding author, e-mail: chakhmou@ms.umanitoba.ca
[2] Department of Geology, Lakehead University, Thunder Bay, Ontario, P7B 5E1, Canada
[3] 594 Main Road, Hudson, Québec, J0P 1H0, Canada

Abstract: Rasvumite and "loparite-(Ce)" from the Mont Saint-Hilaire alkaline complex in Québec were re-examined using a variety of analytical techniques. Rasvumite crystals from a marble xenolith and tawite ("sodalite xenolith") entrained in nepheline syenite contain significant amounts of Rb and Cs (up to 7.2 and 2.6 wt.%, respectively). Our data indicate that these elements are more compatible with respect to rasvumite than sodalite, tainiolite, or perovskite-type phases. Cubo-octahedral crystals and penetration twins of "loparite-(Ce)" from the tawite comprise {100} growth sectors composed of loparite-(Ce) and {111} sectors composed of lueshite; the proportion of $Na_{0.5}Ce_{0.5}TiO_3$ and $NaNbO_3$ components varies by $\geqslant$15 mol.% between the sectors. In addition to the light rare-earth elements and Ti, the {100} sectors are enriched in K, Sr, Ba, Y, Th, U, Fe, Si and Zr with respect to the {111} sectors, which show higher levels of Na, Ca, Nb and Ta. Some elements (Ba, Th and U) exhibit a two-fold or greater difference in *D* between the sectors. Crystal-chemical analysis of the sector zoning indicates that higher-charged cations partition into surface protosites with fewer bonds satisfied (in agreement with Dowty's model). Among isovalent *A*-site cations, the larger partition into the {100} sectors. This observation is at variance with Dowty's predictions, but can be readily explained in terms of the relative differences in bond strength between large and small cations (estimated from their bond-valence parameters). The distribution of *B*-site cations is highly charge-dependent (but size-independent) and constrained mostly by heterovalent substitutions in the *A* site within a given sector. Comparison with the published data shows that the inter-sectorial distribution of cations in the perovskite structure is controlled not only by their charge, radius and involvement in coupled substitutions, but also by the chemistry of crystallization environment (*e.g.*, availability of Nb). The implications of these data for the study of element partitioning in perovskites are discussed. The loparite-lueshite intergrowths and Rb-Cs-rich rasvumite in the tawite are interpreted to have crystallized in equilibrium with sodalite, aegirine and tainiolite from halogen-rich peralkaline magma. The tawite and its host nepheline syenite may have formed from cognate immiscible magmas, as proposed earlier by Piilonen, McDonald and Lalonde.

Key-words: rasvumite, alkali sulfides, loparite-(Ce), lueshite, perovskite, sodalite, sector zoning, trace-element partitioning, tawite, peralkaline rocks, Mont Saint-Hilaire, Québec.

Introduction

The Mont Saint-Hilaire complex (MSH, hereafter) in Québec (Canada) is one of the best-known intrusions of alkaline rocks in the world and a collecting site frequented by both professional and amateur mineralogists. Whereas significant progress has been recently made in the understanding of the crystal chemistry of some ubiquitous rock-forming and accessory minerals from MSH (*e.g.*, Piilonen *et al.*, 1998, 2003), the less-common minerals, for which MSH is not the type locality, have not been studied in adequate detail. To address this deficiency, we undertook a detailed reinvestigation of some of the poorly characterized material from MSH. In the present work, we report new data on rasvumite and perovskite-group minerals (PGrM) from this locality and discuss the petrologic implications of these new data. Some of our findings are relevant to petrologic problems well outside the realm of mineralogically exotic peralkaline rocks.

Analytical methods

The abundances of major elements in rasvumite and PGrM were determined by energy-dispersive X-ray spectrometry (EDS) using a Jeol 5900 scanning-electron microscope (SEM) equipped with a LINK ISIS analytical system, and operated at 20 kV and 0.64–0.66 nA. Raw EDS spectra were acquired for 180 s (live time) and processed using the LINK ISIS-SEMQUANT software, with full ZAF

DOI: 10.1127/0935-1221/2007/0019-1739
0935-1221/07/0019-1739 $ 6.30

Table 1. LA-ICP-MS operating and data-acquisition parameters.

ICP – MS	
Model	Element 2
Forward Power	1374 W
Gas flows:	
Plasma (Ar)	16 L min^{-1}
Auxiliary (Ar)	0.80 L min^{-1}
Sample (Ar/He)	0.649/0.414 (L min^{-1})
LA	
Model	Merchantek LUV 213
Wavelength	213 nm
Repetition rate	10 Hz
Pre-ablation warm-up	none
Pulse duration	5 ns
Spot size	20 μm
Power	65 %
Incident pulse energy	~0.020 mJ
Energy density on sample	~6.22 J cm^{-2}
DataAcquisitionParameters	
Data acquisition protocol	time resolved analysis
Scanning mode	BScan and EScan
Detector mode	analog and counting
Isotopes	^{88}Sr, ^{89}Y, ^{90}Zr, ^{137}Ba, ^{139}La‡, ^{181}Ta, ^{238}U
Dwell time (segment duration)	150 ms
Magnet settling time	0.001–0.3 s
Time/Pass	0.08 s
Runs/Passes*	40/3
Data acquisition(s)	60 s gas blank, 132 s sample ablation

‡ Internal standard.

* A pass is defined as a measurement cycle through the mass spectrum, 3 such passes are averaged and combined into 1 run to create 40 blocks of data per sample.

corrections applied. The following standards were used for the electron-microprobe analysis (EMPA) of rasvumite: chalcopyrite (Fe, S), jadeite (Na), orthoclase (K), synthetic RbCl (Rb) and CsCl (Cs). A Cameca SX 100 fully automated electron microprobe and wavelength-dispersive spectrometry (WDS) were used to confirm that Na, K, Rb, Cs, Fe and S are the only elements present in the MSH rasvumite in detectable quantities (see below).

Several crystals of "loparite-(Ce)" from MSH were examined by EDS in combination with back-scattered electron (BSE) imaging. All of the crystals revealed prominent sector zoning. The orientation of sectors was established by semi-quantitative analysis of carbon-coated faces of uncut crystals, coupled with BSE imaging of oriented offcuts mounted in epoxy. Four crystals were selected for further study, of which two were sufficiently large (~120 μm across) to enable analysis of individual sectors by laser-ablation techniques. Because these crystals exhibited an appreciable core-to-rim compositional variation, two smaller crystals (~50 μm across) with essentially uniform composition *within* the sectors were selected for WDS analysis. This method was chosen because K, Fe and Si could not be quantified accurately by either EDS or laser-ablation techniques. The larger crystals were carefully mapped under BSE and reflected light to enable accurate positioning of a laser beam. The EDS data were obtained with the Jeol 5900 SEM, as described above, but using the following standards: loparite (Na, La, Ce, Pr, Nd, Nb), perovskite (Ca, Ti) and synthetic $ThNbO_4$ (Th). The WDS analyses were done using the Cameca SX 100 instrument (see above) operated at 15 kV and 15 nA, with a beam size of 5 μm. The following standards were employed in the analysis: albite (Na), diopside (Ca, Si), fayalite (Fe), orthoclase (K), synthetic rare-earth phosphates (La, Ce, Pr, Nd and Sm), $SrTiO_3$ (Sr, Ti), Ba-Na niobate (Nb), ThO_2 (Th) and UO_2 (U).

The two large crystals of "loparite-(Ce)" were analyzed for Sr, Ba, Y, U, Zr and Ta by laser-ablation inductively-coupled mass-spectrometry (LA-ICP-MS). Several other elements (Rb, Cs, Lu and Hf) were sought, but found not to be present at detectable levels. Table 1 shows the instrument parameters used for the analyses. La, determined independently by EMPA, was used as an internal standard to monitor ablation. The external calibration standard used was NIST glass 610 with the nominal values reported by Pearce *et al.* (1977). The choice of analytical isotopes was constrained by expectations of sensitivity and the potential for spectral overlaps and molecular interferences. The Element 2 was operated in low-resolution mode and isotopes were carefully chosen to avoid interference from geochemically coherent elements, *e.g.*, between the rare-earth elements (REE) and Ba. Here, ^{137}Ba is free from interference. ^{181}Ta may be potentially interfered by heavy REE. Given that Lu, used to monitor heavy REE, is present in the

examined samples at or below a detection limit of 3 ppm, this potential interference is believed to be negligible. The ^{88}Sr, ^{89}Y and ^{90}Zr values may be affected by argide production in the plasma, and the principal problem lies with Ti argides affecting ^{88}Sr at all resolutions. Argide production for the given tuning conditions was found to be negligible by monitoring ^{88}Sr counts per second while running a series of pure Ti standards. While ^{238}U was free from interferences in this matrix, oxide production (which would reduce sensitivity) was monitored during instrument tuning and kept below 0.3 % of the ^{238}U count rate.

The measured trace element intensities were processed using GLITTER (van Achterbergh *et al.*, 2001). Three standard signals were collected before and after the data acquisition at 9 points. The standard signals were averaged, and local backgrounds used on all signals. The time-resolved portions of the sample signals were selected to gather as large a sample as possible and to keep fractionation below 10 % and the fractionation-to-error ratio at or below 3.

X-ray diffraction (XRD) data for rasvumite and "loparite-(Ce)" were obtained by Gandolfi method using Ni-filtered CuKα gradiation with a 114.6-mm camera mounted on a Phillips 3710 instrument operated at 30 mA and 40 kV. Diffraction lines were measured and indexed manually using the data of Czamanske *et al*. (1979) and Chakhmouradian *et al.* (1999) as references. The cell parameters were refined using the UnitCell software (Holland & Redfern, 1997).

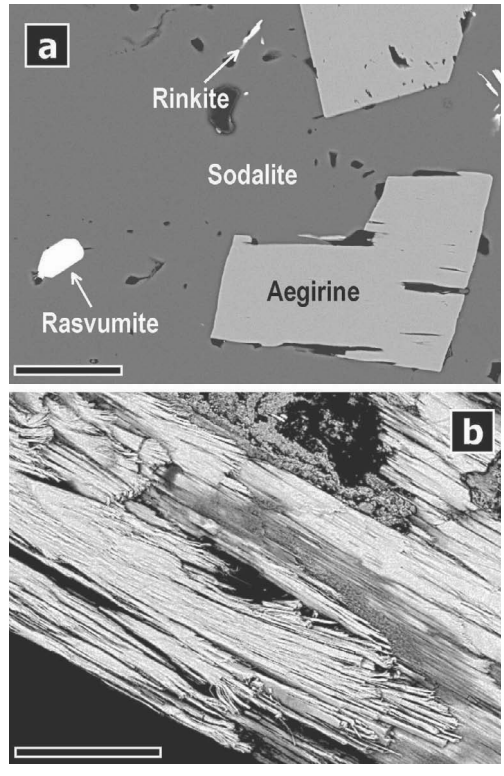

Fig. 1. Morphology of rasvumite from Mont Saint-Hilaire. (a) Euhedral rasvumite (Rsv) included in sodalite (Sdl), other minerals present are aegirine (Ae) and rinkite (Rnk); BSE image. (b) Bladed rasvumite from marble xenoliths showing splintery cleavage and hydrated areas (gray); SEM image. Scale bar is 50 μm for both.

Rb-Cs-bearing rasvumite

Rasvumite is a rare K-Fe sulfide with a chain-like structural motif (*e.g.*, Mitchell *et al.*, 2004). Apart from the type locality at Khibiny in the Kola Peninsula, Russia (Sokolova *et al*., 1970), this mineral has been described from the adjacent Lovozero intrusion, Lake Flekkeren area in Norway, Coyote Peak in California, Point of Rocks in New Mexico, and Oldoinyo Lengai in Tanzania (Czamanske *et al*., 1979; Ifantopulo *et al*., 1983; DeMark, 1984; Jamtveit *et al*., 1997; Jago & Gittins, 1999). At MSH, rasvumite was described first by Horváth & Gault (1990) as encrustations in the so-called "sodalite xenoliths". In 1991, G. Haineault found this mineral in marble xenoliths, where it forms bladed crystals up to 30 mm in length (Horváth & Pfenninger-Horváth, 2000). This material was subsequently examined by Gebhard & Schlüter (1994). With the exception of Mn-F-rich rasvumite from Tanzania, all previously reported compositions approach the ideal formula KFe_2S_3. The analysis of MSH rasvumite by Gebhard & Schlüter (1994) has a low total and yields a non-stoichiometric formula suggesting the presence of additional element(s) substituting for K.

We identified rasvumite in a "sodalite xenolith" of near-spherical shape composed of three concentric zones (from the core outward): (i) villiaumite, (ii) sodalite, and (iii) pectolite. This "xenolith" was found in the Poudrette quarry at the contact between hornfels and nepheline syenite incorporating numerous fragments of marble and sodalite-rich rock (for definitions and descriptions, see Horváth & Gault, 1990; Piilonen *et al.*, 1998; McDonald & Chao, 2004). The nepheline syenite contains a greater proportion of mafic minerals (and, thus, is considerably darker) than leucocratic nepheline syenites comprising the bulk of the East Hill suite. Piilonen *et al.* (1998) proposed that the sodalite-rich parageneses and their host nepheline syenites could have derived from the same parental magma by liquid immiscibility. Our observations support this model and are certainly inconsistent with the identification of these rocks as xenoliths (see Discussion). It is also noteworthy that, regardless of their origin, the sodalite-rich rocks from MSH should not be referred to as sodalite syenite (cf. Piilonen *et al.*, 1998). According to the nomenclature of igneous rocks (Le Maitre, 2002), the term "foid syenite" is reserved for plutonic rocks with a foid-to-feldspar ratio of $\geqslant$1.5 and the preponderance of alkali feldspar over plagioclase ($P' < 10$). The paucity of *any* feldspar in these rocks requires that they be termed sodalitolites or tawites, the latter name alluding to the "type locality" of aegirine-sodalite rocks in the Tavaiok (Tawajok) River valley at Lovozero. The term "sodalite xenolith" is also undesirable because sodalite is not a rock name.

In this sample, rasvumite occurs as minute ($\leqslant$25 μm), nearly equant crystals enclosed in sodalite (Fig. 1a), which is devoid of detectable Ca and contains very little of the nosean component (<0.7 wt.% SO_3). Other minerals found in the same sample include euhedral crystals of

Table 2. Representative compositions and unit-cell parameters of rasvumite from Mont Saint-Hilaire.

	bladed		equant			bladed		equant	
	1	2	3	4		1	2	3	4
Elements, wt.%:					Formulae calculated to a total of 6 atoms:				
Na	0.10	0.17	0.13	0.14	Na	0.011	0.019	0.014	0.016
K	14.63	14.34	11.76	11.42	K	0.953	0.926	0.765	0.750
Rb	2.43	3.13	6.75	7.15	Rb	0.072	0.092	0.201	0.215
Cs	0.42	0.49	2.26	2.62	Cs	0.008	0.009	0.043	0.051
Fe	43.39	43.72	42.67	42.52	Fe	1.979	1.976	1.944	1.955
S	37.46	37.82	38.21	37.62	S	2.976	2.978	3.032	3.013
Total	98.43	99.67	101.78	101.47					
Unit-cell parameters:									
a, Å	9.025(13)								
b, Å	11.023(3)								
c, Å	5.435(6)								
V, Å^3	540.7(16)								

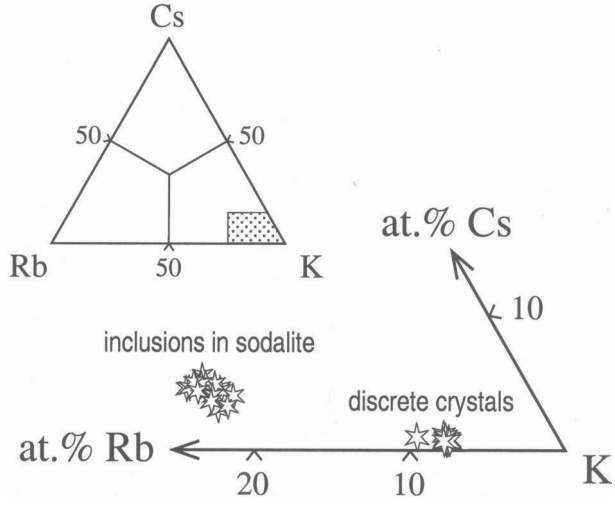

Fig. 2. Composition (at.%) of rasvumite from Mont Saint-Hilaire.

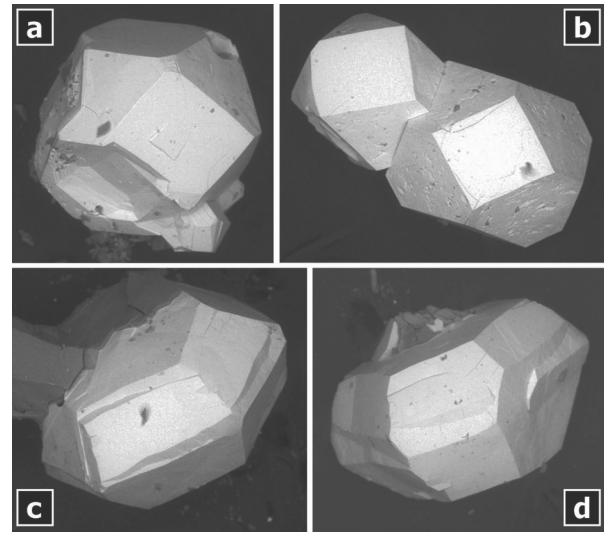

Fig. 3. Morphology of "loparite-(Ce)" crystals and intergrowths from Mont Saint-Hilaire. SEM images. (a, b) Randomly intergrown cubo-octahedral crystals; (c, d) "flying saucer" penetration twins with {111} as the principal form.

aegirine-augite zoned to aegirine, villiaumite, intergrowths of loparite-(Ce) with lueshite (see below), manganoan pectolite, niobian rinkite, galena, and a lithian mica compositionally intermediate between tainiolite (*ca.* 60 mol.%) and phlogopite+annite. In this paragenesis, pectolite occurs only as inclusions in aegirine, whereas sodalite is fractured at the contact with, and veined by, villiaumite. Small angular fragments of sodalite and clinopyroxene are embedded in villiaumite. The clinopyroxene, mica, rasvumite and loparite-lueshite intergrowths appear to be in equilibrium with the sodalite.

Rasvumite from this paragenesis contains up to 7.2 wt.% Rb and 2.6 wt.% Cs (Table 2). The presence of Rb and Cs in the MSH rasvumite was confirmed by WDS, but the lack of a suitable standard precluded its accurate analysis. Using wavelength (sinθ) scans, we also confirmed the absence in these samples of other elements that could potentially substitute for K (Ba, Sr, Tl and Pb) or Fe (Cu, Mn and Ni). Both sodalite and tainiolite were also analyzed by WDS, but Rb and Cs were not detected in either of these minerals.

For comparative purposes, we also re-examined the bladed rasvumite of Horváth & Gault (1990). This material is chemically heterogeneous due to pervasive alteration along cleavage planes (Fig. 1b). The altered areas appear to be enriched in Fe and H_2O relative to the nominal composition KFe_2S_3. Fresh areas contain elevated levels of Rb and Cs (up to 3.1 and 0.6 wt.%, respectively). Note that without these elements, the analytical totals (Table 2) would be close to the value reported by Gebhard & Schlüter (1994). Thus, our data indicate significant solubility between KFe_2S_3 and $RbFe_2S_3$ in natural rasvumite (Fig. 2); complete miscibility among the synthetic K, Rb and Cs end-members has been established by Mitchell *et al.* (2004). The XRD pattern and unit-cell parameters of the bladed variety (Table 2) are virtually indistinguishable from the previously reported data (*e.g.*, Czamanske *et al.*, 1979).

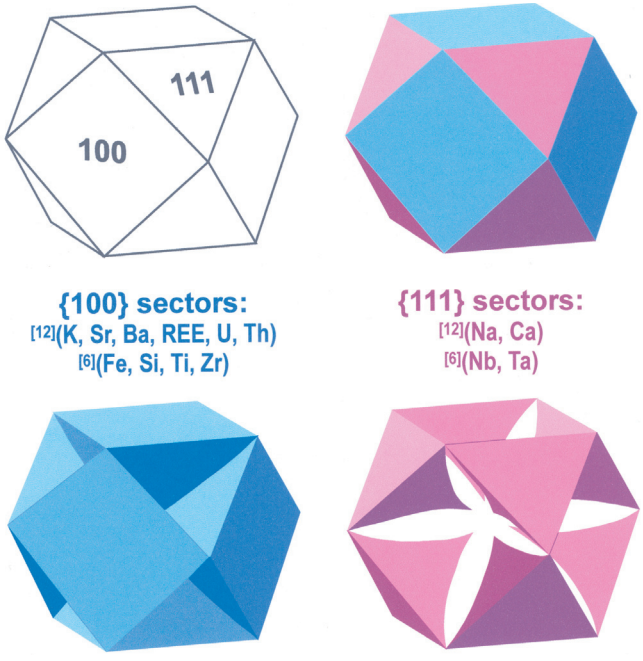

Fig. 4. Anatomy of sector-zoned "loparite-(Ce)" crystals from Mont Saint-Hilaire. {100} sectors (blue) show the preponderance of $Na_{0.5}LREE_{0.5}TiO_3$ component, whereas {111} sectors (purple) contain a higher proportion of $NaNbO_3$ and, thus, should be termed lueshite.

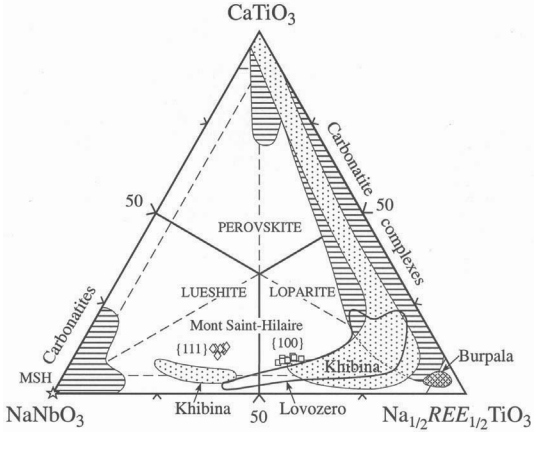

Fig. 5. Composition (mol.%) of perovskite-group minerals from Mont Saint-Hilaire and other alkaline complexes. Note large compositional difference between the {100} and {111} sectors in the Mont Saint-Hilaire material. The diagram was adopted from Chakhmouradian *et al.* (1999) with minor additions and alterations.

Sector-zoned "loparite-(Ce)"

At MSH, the most common PGrM is lueshite approaching the ideal composition $NaNbO_3$. The intergrowths studied in the present work were originally described as loparite-(Ce) (Wight & Chao, 1995). They are associated with the equant rasvumite, and occur as cubo-octahedral crystals up to a few hundred μm across, random intergrowths of such crystals and penetration twins of hexagonal tabular habit (Fig. 3). This habit results from {111} being the dominant crystal form, unlike in the more common fluorite-law twins composed of cubes. Both crystals and twins comprise sectors of different average atomic number (AZ). The high-AZ sectors, corresponding to the {100} form, contain higher levels of light REE (LREE), Sr, Th, Ti and Fe than the {111} sectors; the latter are comparatively enriched in Na, Ca and Nb (Tables 3, 4, Fig. 4). The {111} sectors do not reach the center, indicating that the crystal habit was initially cubic. Their outward-flaring shape (Fig. 4) suggests that the growth rate of octahedral faces decelerated relative to that of the cubic faces. Locally, subtle oscillatory zoning is superposed on the sectorial pattern. In both {100} and {111} sectors, the proportion of Na and Nb decreases, and that of Ca slightly increases outward.

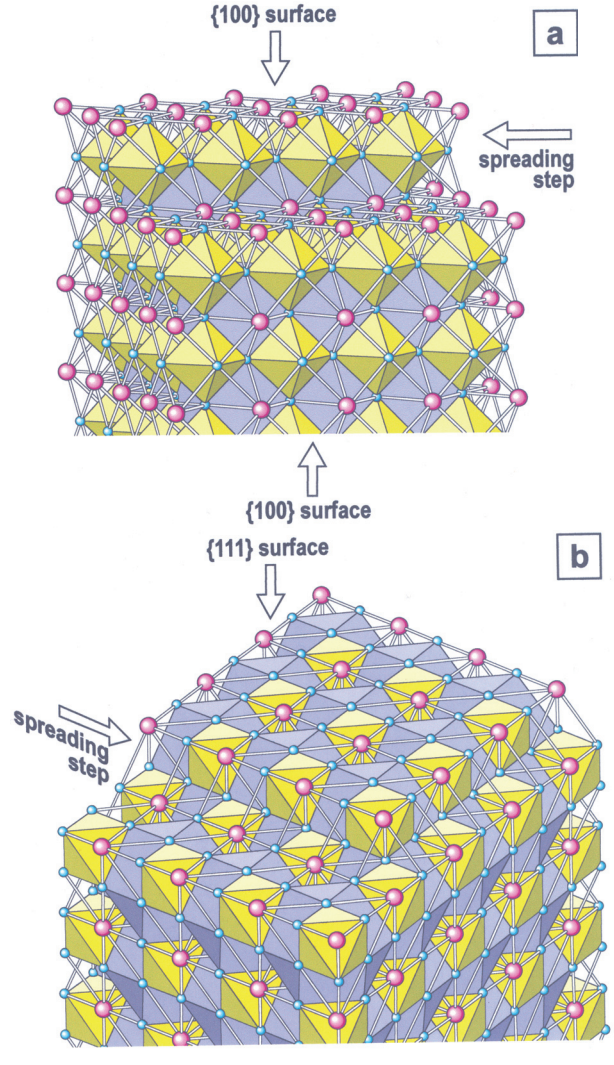

Fig. 6. Morphology and *A*-site bonding topology of growing loparite crystal: (a) ⟨100⟩ growth step and terraces on the {100} face; (b) ⟨110⟩ step and terraces on the {111} face. *A*-site cations attached to the surface are indicated by purple spheres; their bonding configurations relative to anions (small blue spheres) are shown by spokes. For clarity, the bulks of crystals are shown to consist of complete AO_{12} polyhedra (lavender) and BO_6 octahedra (yellow). See text for further discussion.

A single LA-ICP-MS analysis from the core of one of the crystals gave a Ta/Nb value slightly higher than those near the rim in the cubic and octahedral sectors (0.018, 0.015 and 0.012, respectively).

The compositions of MSH crystals can be expressed in terms of three end-member components: loparite, lueshite and perovskite (Fig. 5), and plot near the most evolved compositions from Khibiny and Lovozero, but are somewhat richer in Ca. In accord with the existing nomenclature, the cubic cores and {100} growth sectors correspond to loparite-(Ce), whereas the {111} sectors to lueshite or isolueshite. Distinction between the latter two minerals is impossible without a single-crystal diffraction study. Given that all $NaNbO_3$-dominant compositions from "sodalite xenoliths" examined to date correspond to pseudocubic lueshite (Mitchell *et al.*, in prep.), we shall refer to the material in the Na-Nb-enriched sectors as lueshite. Geometric distortion of the archetypal perovskite structure (space group *Pm*3*m*) does not necessarily produce superlattice diffraction lines detectable with conventional powder-diffraction techniques. From the absence of superlattice lines in the XRD pattern of loparite-lueshite intergrowths, we conclude that departure from the undistorted cubic structure is negligible; the measured unit-cell parameter is also in excellent agreement with that calculated from the ionic radii assuming the ideal *Pm*3*m*-type atomic arrangement (Table 3).

Both cation charge and radius are crucial to the development of sector zoning (*e.g.*, Dowty, 1976; Paquette & Reeder, 1995; Cressey *et al.*, 1999). To examine the effect of ionic radius on cation distribution in the MSH material, we determined the content of trace elements isovalent with, but differing in size from, the major cations (Tables 3, 4). These elements included K^{1+}, Rb^{1+} and Cs^{1+} (all larger than Na^{1+}), Sr^{2+} and Ba^{2+} (both larger than Ca^{2+}), Y^{3+} (smaller than $LREE^{3+}$), U^{4+} (smaller than Th^{4+}), Si^{4+} and Zr^{4+} (smaller and larger than Ti^{4+}, respectively). From Tables 3 and 4, it is obvious that Y^{3+} and U^{4+} behave similarly to the other high-charge cations, *i.e.* partition into the {100} sectors. The small-cation to large-cation mass ratios are essentially identical in the {100} and {111} sectors (U/Th value is but marginally higher in the latter). The mono- and divalent cations exhibit a remarkably different distribution pattern: Na^{1+} and Ca^{2+} are enriched in the {111} sectors, whereas K^{1+}, Sr^{2+} and, especially, Ba^{2+} in the {100} sectors. The K/Na, Ba/Ca, Ba/Sr and Sr/Ca ratios are consistently higher in the latter (Tables 3, 4). The minor *B*-site cations show a radius-independent charge-controlled distribution (*i.e.*, Si and Zr partition into the Ti-enriched {100} sectors whereas Ta into the {111} sectors: Tables 3, 4).

Sector zoning has been previously documented in PGrM from different igneous rocks, but is especially common in peralkaline parageneses. Some examples include tausonite (Vorob'yov *et al.*, 1987), perovskite (Dawson & Hill, 1998), loparite (Bussen & Sakharov, 1972), and complex intergrowths of perovskite and loparite (Mitchell & Chakhmouradian, 1999). These examples cover a wide range of compositions in terms of their Na, Ca, Sr, LREE, Th, Nb and Ti contents. Unfortunately, only two of the published descriptions contain any information on the crystallographic orientation of individual sectors (Vorob'yov *et al.*, 1987; Mitchell & Chakhmouradian, 1999). On the basis of the EMPA data and BSE image provided by Dawson & Hill (1998), the high- and low-AZ zones in their sample can be confidently identified as cubic and octahedral growth sectors, respectively. Comparison of our data with those from the literature shows that LREE, Th, Sr, K, Fe, Si and Ba (where detected) are invariably concentrated in the {100} sectors, whereas Ca and Nb (where detected) in the {111} sectors (Table 5). The K/Na and Sr/Ca values are consistently higher in the {100} sectors.

Discussion

Origin of the sodalite-rich "xenolith"

The peralkaline sodalite-rich rock, containing Rb-Cs-rich rasvumite and loparite-lueshite intergrowths, shows textural characteristics distinguishing it from bona fide xenoliths. The observed relationships among the three major minerals indicate that the peripheral pectolite zone formed before the intermediate sodalite zone, which, in its turn, was succeeded by villiaumite in the core. Such crystallization order points to an origin other than the entrapment of a fragment of sodalite-rich rock in nepheline-syenitic magma and their subsequent reaction to produce the marginal zone of pectolite. The lack of any mineralogical or textural evidence of metasomatism (such as pseudomorphs, shadow structures, coronas of fibrous amphibole around clinopyroxene, etc.) is also inconsistent with a xenolithic origin, because xenoliths in alkaline rocks are typically metasomatized. A more plausible explanation is that this unusual mineral assemblage crystallized from an enclave of peralkaline magma extremely rich in volatiles (F, Cl and SO_3) *during* or *following* the emplacement of the host nepheline syenite. Because of the scarcity of the material available to us, neither the origin of this hypothetical melt nor its genetic relationships with the nepheline syenite could be established with certainty. On the basis of field evidence and clinopyroxene compositions, Piilonen *et al.* (1998, p. 789) proposed that the two rock types may have been derived from a single parental magma by liquid immiscibility. This model is consistent with our observations and the available (albeit, limited) experimental data (Kogarko *et al.*, 1974; Romanchev & Kuznetsova, 1982; Yudintsev *et al.*, 1983). Immiscible separation of a Na-halogen-rich melt has also been invoked to explain the occurrence of sodalite-rich parageneses in alkaline rocks at Lovozero in the Kola Peninsula (Gerasimovskii *et al.*, 1968a, pp. 169-170), Gran Canaria (Romanchev & Kuznetsova, 1982), and Junguni in Malawi (Woolley & Platt, 1988).

The enrichment of the MSH rasvumite in Rb and Cs (Table 2), and the low Ta/Nb ratio of the "loparite" (Table 3) both indicate that their parental melt was extremely evolved. The association of Rb and Cs with fractionated granitic pegmatites is well known (*e.g.*, Černý, 1982), but in silica-undersaturated agpaitic rocks (*i.e.* those not associated with peralkaline granites), minerals containing these

Table 3. Representative compositions of large "loparite-(Ce)" crystals.

	{100} sectors		{111} sectors			{100} sectors		{111} sectors	
	1	2	3	4		1	2	3	4
Oxides, wt.%:					Formulae calculated to 3 atoms of oxygen:				
Na_2O	11.28	10.70	13.11	12.87	Na	0.628	0.608	0.719	0.696
CaO	2.79	2.70	3.30	3.85	Ca	0.086	0.085	0.100	0.115
La_2O_3	6.15	6.24	4.59	3.92	La	0.065	0.068	0.048	0.040
Ce_2O_3	12.58	13.24	8.67	8.97	Ce	0.132	0.142	0.090	0.092
Pr_2O_3	0.66	0.94	1.12	0.79	Pr	0.007	0.010	0.012	0.008
Nd_2O_3	2.19	1.83	1.38	1.88	Nd	0.022	0.019	0.014	0.019
ThO_2	6.49	7.05	3.06	3.32	Th	0.042	0.047	0.020	0.021
					ΣA	0.982	0.979	1.003	0.991
TiO_2	29.90	28.82	22.58	24.48	Ti	0.646	0.636	0.481	0.513
Nb_2O_5	27.21	26.78	40.42	39.08	Nb	0.353	0.355	0.518	0.492
					ΣB	0.999	0.991	0.999	1.005
Total	99.25	98.30	98.22	99.16					
Elements, ppm:					Mol.% major components (range):				
Sr	1942(171)		1476(220)		$Na_{0.5}Ce_{0.5}TiO_3$	44.8-48.5		29.7-33.9	
Ba	1552(242)		208(77)		$NaNbO_3$	30.8-37.6		49.0-52.0	
La	53686(592)		34278(1308)		$CaTiO_3$	7.7-10.0		10.0-12.2	
Y	18(3)		12(3)		$Th_{0.5}TiO_3$+				
U	190(14)		98(11)		$Na_{0.67}Th_{0.33}TiO_3$	8.9-11.8		4.2-8.9	
Zr	312(123)		224(39)						
Ta	2689(452)		3449(674)						
Element ratios (mass):					Unit-cell parameter, Å:				
Sr/Ca	0.094(8)		0.054(8)		measured		3.897(3)		
Ba/Ca	0.075(12)		0.008(3)						
Ba/Sr	0.76(7)		0.17(7)		calculated‡	3.885		3.901	
Y/La	0.00032(6)		0.00035(8)		calc. average‡		3.892‡		
Y/Nd	0.0010(2)		0.0009(2)						
U/Th	0.0030(2)		0.0036(4)		Calculated sector-average bond distances, Å:				
Zr/Ti	0.0017(7)		0.0015(3)		*A*-O	2.747		2.758	
Ta/Nb	0.015(2)		0.012(2)		*B*-O	1.942		1.950	

Points (1) and (3) are near the center of the intergrowth, points (2) and (4) are closer to the edge. Oxides by EMPA, elements by LA-ICP-MS; LA-ICP-MS data are averages of 4 analyses each. n.d = not detected; element ratios are based on the average compositions of {100} and {111} sectors determined by EMPA and LA-ICP-MS.

‡ Calculated using ionic radii of Shannon (1976), the average calculated assuming 60 % of the crystal volume occupied by {100} sectors and 40 % by {111} sectors.

elements in significant concentrations are exceedingly rare. In alkaline plutons with a well-established sequence of crystallization (*e.g.*, Lovozero), the whole-rock abundances of Rb and Cs in the major intrusive series increase with fractionation (Gerasimovskii *et al.*, 1968b). However, even in the most evolved parageneses at Lovozero, MSH and similar complexes, such minerals as astrophyllite and leifite, known for their structural tolerance toward large alkali cations, contain <1 wt.% Rb and Cs (Sokolova *et al.*, 2002; Piilonen *et al.*, 2003). The rasvumite described in the present paper is unique in containing very high levels of these elements. Interestingly, our data seem to indicate that Rb and Cs are much more compatible with respect to rasvumite than Li-Mg mica, sodalite or PGrM (see above). This conclusion is somewhat unexpected, given high percentages of Rb and Cs in trioctahedral mafic micas from fractionated granitic pegmatites (*e.g.*, Černý *et al.*, 2003). One significant implication of these observations is that K sulfides may be an important sink for Rb and Cs in (hyper)agpaitic parageneses. Evidently, rasvumite and similar phases (*e.g.*, djerfisherite, bartonite and murunskite) should be routinely analyzed for Rb and Cs.

The Ta/Nb ratio in oxide minerals, including PGrM, decreases progressively with fractionation. For example, at Lovozero, loparite from the most primitive foid syenites has a Ta/Nb ratio ⩾0.06 (*i.e.* close to, or higher than, the primitive-mantle value: McDonough & Sun, 1995), whereas the most evolved agpaitic parageneses

Table 4. Average composition of small "loparite-(Ce)" crystals.

	{100} sectors		{111} sectors			{100}	{111}
	average	e.s.d	average	e.s.d.		sectors	sectors
Oxides, wt.%:					Formulae calculated to 3 atoms of oxygen:		
Na_2O	11.57	0.20	13.15	0.11	Na	0.632	0.703
K_2O	0.05	0.01	0.01	0.01	K	0.002	-
CaO	3.05	0.03	4.17	0.04	Ca	0.09	2 0.123
SrO	0.12	0.01	0.05	0.01	Sr	0.002	0.001
La_2O_3	6.35	0.10	4.38	0.21	La	0.066	0.045
Ce_2O_3	12.60	0.26	8.76	0.20	Ce	0.130	0.088
Pr_2O_3	0.67	0.06	0.51	0.08	Pr	0.007	0.005
Nd_2O_3	2.79	0.20	1.93	0.12	Nd	0.028	0.019
Sm_2O_3	0.07	0.06	0.07	0.04	Sm	0.001	0.001
ThO_2	5.42	0.24	2.33	0.06	Th	0.035	0.015
UO_2	0.03	0.02	0.01	0.01	U	-	-
					Σ*A*	0.995	1.000
Fe_2O_3	0.09	0.04	0.05	0.02	Fe	0.002	0.001
SiO_2	0.81	0.06	0.01	0.02	Si	0.023	-
TiO_2	31.67	0.28	25.56	0.21	Ti	0.671	0.530
Nb_2O_5	24.53	0.57	38.41	0.40	Nb	0.312	0.479
					Σ*B*	1.008	1.010
Total	99.82		99.40				
Element ratios (mass):					Mol.% major components (average):		
K/Na	0.0045(9)		0.0010(7)		$Na_{0.5}Ce_{0.5}TiO_3$	46.3	31.6
K/Ca	0.018(3)		0.003(2)		$NaNbO_3$	31.2	47.9
Nd/La	0.44(3)		0.44(4)		$CaTiO_3$	9.2	12.3
Fe/Ti	0.0035(15)		0.0021(8)		$Th_{0.5}TiO_3$+		
Si/Ti	0.020(1)		<0.001		$Na_{0.67}Th_{0.33}TiO_3$	9.0	3.4

These data were derived by averaging 5 point analyses for each {100} and {111} sectors.
* Total Fe given as Fe_2O_3.

Table 5. Sector-zoned perovskite-group minerals: Selected element ratios.

Mineral	Elementr atios (mass)								
Locality (rock type)	K/Na	K/Ca	Sr/Ca	Ba/Ca	La/Ca	Th/Ca	Nb/Ti	Fe/Ti	Si/Ti
Loparite-(Ce) – lueshite									
Mont Saint-Hilaire, Québec (tawite) [1]									
{100} sectors	0.004	0.018	0.09	0.08	2.5	2.2-3.0	0.9-1.0	0.004	0.020
{111} sectors	0.001	0.003	0.05	0.01	1.3	0.7-1.0	1.8-1.9	0.002	<0.001
Tausonite									
Murun, eastern Siberia (lamprophyllite-aegirine veins) [2]									
{100} sectors	0.10	0.15	16.8	0	2.02	n.a	n.a	0.010	0.030
{111} sectors	0.04	0.04	11.2	0	1.24	n.a	n.a	0.006	0.003
Perovskite									
Oldoinyo Lengai, Tanzania (combeite-lamprophyllite nephelinite) [3]									
{100} sectors	0.033	0.015	0.85	0.054	0.63	0.042	0.22	0.020	<0.001
{111} sectors	0.030	0.009	0.66	0.020	0.37	0.022	0.23	0.019	<0.001
Loparite-(Ce) – perovskite									
Hills Pond, Kansas (olivine lamproite) [4]									
{100} sectors	0.32	0.049	0.28	n.a	0.23	0.022	0.021	0.008	0.017
{111} sectors	0.11	0.008	0.14	n.a	0.05	0.005	0.034	0.006	0.003

n.a = no data available
References: [1] this work; [2] Vorob'yov *et al.* (1987); [3] Dawson & Hill (1998); [4] Mitchell & Chakhmouradian (1999).

contain loparite and lueshite with Ta/Nb $\leqslant 0.02$ (Mitchell & Chakhmouradian, 1996; Chakhmouradian & Mitchell, 2002a), *i.e.* similar to the compositions documented in the present work. The core-to-rim decrease in Ta/Nb value, documented in the MSH material, is consistent with liquidus crystallization (Chakhmouradian, 2006).

The acicular rasvumite, containing moderate levels of Rb and Cs, occurs in a "hyperagpaitic" mineral assemblage (with carbonates, fluorite and sulfides) in marble xenoliths (Horváth & Pfenninger-Horváth, 2000). Neither the timing of this type of mineralization nor the provenance of fluids, which produced it, is presently known. Carbonate- and F-rich fluids are a common product of evolution of alkaline magmas (*e.g.*, Chakhmouradian & Mitchell, 2002b; Pekov & Podlesnyi, 2004), and could have sourced from either tawites or nepheline syenites.

Sector zoning in perovskite-group minerals: crystal-chemical controls

The origin of sector zoning in PGrM has not been previously discussed to any significant extent. One important observation that can be made from the published and our own data is that variations in the proportion of different *A*-site cations (especially, Na, LREE, Ca and Sr) are generally much more pronounced than variations in the proportion of *B*-site cations (see Table 3 for site designations). In fact, the MSH material is the only known example of dramatic (0.13–0.17 apfu) inter-sectorial differences in the occupancy of *B* site. Thus, it seems reasonable to seek an explanation to the observed zoning in the structural setting and characteristics of *A*-site cations, and then explore possible mechanisms of *B*-cation partitioning between the sectors.

Numerous studies of zoning in other minerals offer various explanations for the crystallographically controlled partitioning of elements within a crystal (for comprehensive discussions, see Shearer & Larsen, 1994; Watson & Liang, 1995). Among the possible mechanisms and driving forces, we can confidently rule out the following:

(1) Interplay between the different rates of ion diffusion in the melt, and growth or lateral layer-spreading rates of crystal forms (Wass, 1973; Paterson & Stephens, 1992; Skulski *et al.*, 1994). In our case, the relatively faster-growing {100} sectors contain higher amounts of less mobile LREE and Th, which is inconsistent with this kinetic model;

(2) rapid crystallization (Kouchi *et al.*, 1983; Brophy *et al.*, 1999). None of the minerals in the tawite "xenolith" show any morphological evidence of rapid crystallization. On the contrary, minerals that commonly exhibit an acicular habit (aegirine-augite, pectolite and rasvumite) here form nearly equidimensional crystals, and the aegirine-augite is devoid of sector zoning so typical of clinopyroxenes from extrusive alkaline rocks (Gamble, 1984; Dobosi *et al.*, 1991);

(3) different lattice-diffusion rates of the cations responsible for zoning (Watson & Liang, 1995). The pattern observed in the MSH sample involves significant variations in the proportion of such weakly bonded and readily diffusing cations as Na^{1+}(cf. Chakhmouradian *et al.*, 1999);

(4) various degree of cation order on symmetrically non-equivalent growth surfaces (Akizuki, 1981, 1984). Detailed structural investigations have not revealed any evidence of cation order in PGrM of different chemistry (*e.g.*, Hu *et al.*, 1992; Mitchell *et al.*, 2000).

Hence, we interpret the observed zoning as a growth feature arising from the differing cation-bonding geometries of {100} and {111} surfaces, in combination with sector-controlled compensation of charge imbalance (*e.g.*, Dowty, 1976). From the available XRD data (see above), we infer that the cubic perovskite structure can serve as a satisfactory model for our analysis. The bonding of *A*-site cations to oxygen atoms on the {100} and {111} surfaces of a loparite crystal is shown in Fig. 6. Given that both {100} and {111} are F forms, the growth probably occurred by layer spreading (Hartman, 1973), which is consistent with the locally observed oscillatory zoning. We further simplified our model by disregarding any relaxation effects that could change the topology and stoichiometry of the surface (Noguera, 2000), and by assuming that (i) the growth steps are parallel to the edges of the corresponding crystal form; (ii) the thicknesses of growth steps on the {100} and {111} surfaces are equal to d_{100} and d_{111}, respectively; and (iii) crystallographic sites, whose bonding requirements are $\geqslant$80 % satisfied, are stably occupied. The latter condition is somewhat arbitrary, and is introduced here to eliminate from consideration the protosites at the base of a step. Note that a step with a large number of vacancies at its base will not be able to spread. Our 80 % bonding requirement is also in accord with Dowty's (1976, p. 461) suggestion that "a 5/6 site … is probably very close to the configuration within the crystal". Surface-relaxation effects are not considered here because the experimental data available for different perovskite-type structures in the literature are either inconclusive or at variance with theoretical predictions (Noguera, 2000).

As shown in Fig. 6, *A*-site cations on the {100} surfaces are less strongly bonded in comparison with the {111} surfaces. Along the edge of a spreading step, where most of the "construction" takes place (*e.g.*, Wang & Ehrlich, 1991), the *A*-site cation is coordinated by 5 and 7 oxygens on the {100} and {111} surfaces, respectively (Fig. 6). In the compositional range determined for the MSH material, this difference corresponds to 0.14–0.51 valence units (v.u.), calculated for the average *A*-O distance of 2.75–2.76 Å (Brown, 1996). On a terrace above or below the step, the difference in bonding is less significant for the two structural settings, but still amounts to 0.06–0.21 v.u.. Tri- and tetravalent *A*-site cations differ from Na^{1+} by about 0.06–0.14 v.u. and from Ca^{2+} by 0.02–0.10 v.u. per bond. These differences imply that LREE, Th and U should partition strongly into the {100} sectors, whereas Na into the {111} sectors, provided that charge balance within the sectors is maintained. This prediction is in accord with the observed cation distribution (Tables 3, 4). Our finding, that the large K^{1+}, Sr^{2+} and Ba^{2+} cations are enriched in the

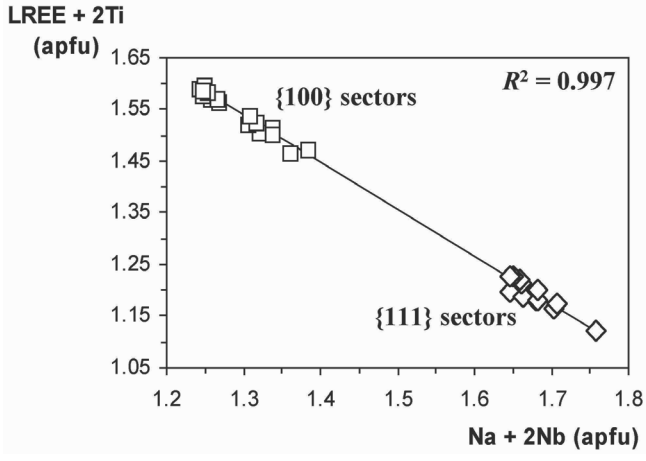

Fig. 7. Inter-sectorial variations in the contents of major cations across the loparite-lueshite intergrowths from Mont Saint-Hilaire. Note high degree of correlation between the heterovalent substitutions in the *A* and *B* sites.

{100} sectors in PGrM from MSH and other localities (see above), is at variance with the prediction of Dowty (1976) that higher-charged *and smaller* cations will be enriched in relatively underbonded protosites. This partitioning behavior can be explained by the fact that, in most PGrM, K, Sr and Ba are trace elements that have to adjust to the lattice dimensions constrained by the major cations (primarily, Na, Ca and LREE). In the range of *A*-O distances calculated for the MSH samples, these trace elements have v.u. values higher than, or comparable to, those of $LREE^{3+}$, Th^{4+} and U^{4+}. Thus, the large mono- and divalent cations will bond to the "underbonded" {100} surfaces as firmly as lanthanides or actinides and will not be as easily detached as Na^{1+} or Ca^{2+}. Although neither Rb nor Cs is present in the studied material at detectable levels (~15 ppm), it is reasonable to expect that these elements will mimic the behavior of large divalent cations.

An antipathetic correlation between LREE (or Th) and Na (or Ca) indicates that, in the MSH samples, charge compensation within the sectors involves substitutions in the *B* site, rather than simple coupled substitutions in the adjacent *A* positions within the same layer (such as $LREE^{3+} + Na^{1+} \Leftrightarrow 2Ca^{2+}$). Analysis of inter-element correlations shows that, in our case, the most important compensation mechanism is $LREE^{3+} + 2Ti^{4+} \Leftrightarrow Na^{1+} + 2Nb^{5+}$ (Fig. 7). This previously unrecognized mechanism requires that the intake of excess Na by a spreading ⟨110⟩ step be accompanied by preferential incorporation of Nb (and trace Ta) in the following growth layer. Such coupled substitutions involving *A* and *B* sites effectively avoid over- or underbonding of surface oxygen atoms. Principally similar models, involving coupled substitutions in successive growth layers, have been proposed to explain charge-controlled substitutions in sector-zoned clinopyroxenes (Dowty, 1976; Skulski *et al.*, 1994; Jensen, 2000).

The Ti^{4+} cation is smaller than either Nb^{5+} or Zr^{4+} in an octahedral coordination, whereas Si^{4+} is significantly smaller than any other *B*-site cation (Shannon, 1976). Hence, the preferential partitioning of Si and Zr into the same sectors as Ti (Tables 3, 4) further indicates that the distribution of these elements was controlled primarily by charge-compensation requirements and not by the differences in cation radius. The inter-sectorial decoupling of penta- and tetravalent *B*-site cations could have been facilitated by the different bonding geometries of *B* protosites exposed on the {100} and {111} surfaces. The *B* protosites exposed on the {111} surfaces have only 50 % of their bonding requirements satisfied (*i.e.* three out of six *B*-O bonds remain available for bonding), in contrast to 80 % for the *B* protosites on the {100} surfaces. It is difficult to assess the relative importance of bonding vs. charge-compensation constraints in this case, because they both promote enrichment of Nb and Ta in the {111} sectors. Partitioning of Fe^{3+} into the {100} sectors (Table 4) is consistent with this model, as it allows local compensation of excess positive charge arising from the enrichment of these sectors in $LREE^{3+}$. Also, a Fe^{3+} cation forms weaker bonds with oxygen atoms in comparison with tetra- or pentavalent cations and, thus, can be more easily detached from the "underbonded" {111} growth surfaces than from the {100} surfaces.

From the above synthesis, it is clear that the inter-sectorial partitioning of a cation is constrained not only by the surface characteristics of a growing crystal, but also by the distribution of *other* cations within, or immediately below, the growth layer (*cf.* Dowty 1976). Coupled substitutions in the same growth layer and successive layers seem equally important. For example, variations in Na and LREE contents in the Hills Pond perovskite are largely controlled by the replacement of Ca^{2+} with Na^{1+} plus $LREE^{3+}$ in the *A* site (Mitchell & Chakhmouradian, 1999), whereas the MSH crystals exhibit a more complex relationship involving substitutions in both *A* and *B* sites (Fig. 7).

Sector zoning in perovskite-group minerals: environmental controls

Comparison of our data with those available in the literature shows that the distribution of Na and Ti in sector-zoned PGrM is strongly dependent on their Nb content (Table 5). In Nb-poor compositions, Na is concentrated in the LREE-rich {100} sectors or shows no appreciable variation between the two sector types, whereas Ti is slightly enriched in the {111} sectors owing to the preferential incorporation of Fe and Si in the cubic sectors. In Nb-rich PGrM, Na is enriched in the {111} sectors concomitantly with Nb and antipathetically with Ti. This seemingly "inconsistent" partitioning behavior of Na is readily explained if we recall that this element is incorporated in the perovskite structure via two principal substitution mechanisms: $Na^{1+} + LREE^{3+} \Leftrightarrow 2(Ca^{2+}, Sr^{2+})$ and $Na^{1+} + Nb^{5+} \Leftrightarrow (Ca^{2+}, Sr^{2+}) + Ti^{4+}$. In the absence of Nb, variations in LREE content between the {100} and {111} sectors will control the distribution of Na, as dictated by charge-compensation requirements. The availability of Nb in other systems will facilitate the enrichment of Na and depletion of Ti in the {111} sectors (as seen in the MSH samples). This example demonstrates the effect of

trace elements (Nb, in our case) on the partitioning of major elements (Na). It is well known that mineral-melt distribution coefficients (*D*) are dependent on the melt composition (*e.g.*, Simon *et al.*, 1994; Taura *et al.*, 2001). The influence of the chemistry of crystallization environment on the intersectorial element partitioning has been reported for a few minerals (*e.g.*, ankerite: Searl, 1990), but, in general, remains poorly understood.

Sector zoning in perovskite-group minerals: petrologic implications

PGrM are the most volumetrically significant constituent of the Earth. The lower mantle is believed to comprise as much as 78–79 wt.% of $MgSiO_3$ and 5–6 wt.% of $CaSiO_3$ (Wood, 2000; Hirose *et al.*, 2004). The distribution of non-silicate PGrM in the mantle is not as well understood, but the published xenolith studies indicate that perovskite-type titanates may be important sinks for LREE, Sr and Nb in the upper mantle (Haggerty 1987; Kopylova *et al.*, 1997). Perovskite *sensu stricto* is an important component of silica-undersaturated crustal rocks and refractory inclusions in meteorites (Grossman, 1980; Chakhmouradian & Mitchell, 1997). It was also postulated to be one of the earliest phases to condensate from the solar nebula (Grossman, 1972). The understanding of element partitioning between PGrM and melts or co-existing minerals is of profound importance to the interpretation of fractionation processes in the primordial Earth (Hirose *et al.*, 2004), interpretation of seismic discontinuities (Wood, 2000) and identification of potential heat sources in the lower mantle (Taura *et al.*, 2001), distinguishing between the postulated nebular and igneous perovskite in meteorites (Simon *et al.*, 1994), constraining $f(O_2)$ in the magma (Lloyd *et al.*, 1996), and many other petrologic problems whose detailed discussion is beyond the scope of this work.

To date, only a few of the analytical studies of element partitioning in PGrM have recognized disequlibrium partitioning as a potential source of discrepancies in the reported data (*e.g.*, Simon *et al.*, 1994). The example of MSH crystals shows that disequilibrium partitioning in relatively slow-cooled systems is capable of producing manifold variations in *D* values for certain elements within a single crystal. It is commonly argued by experimentalists that compositional heterogeneities arising from disequilibrium should be readily detectable in BSE images. Note, however, that the elements showing the largest variation in *D* values between the {100} and {111} sectors (Ba, Th and U) are typically present in both natural and synthetic perovskites in trace quantities. Such substituents as Na, LREE, Sr and Nb are generally abundant in crustal PGrM, but occur at 10^{0-3} ppm levels in high-pressure (Mg, Fe)SiO_3 and $CaSiO_3$ (*e.g.*, Hirose *et al.*, 2004). Evidently, heterogeneities in the distribution of trace elements will not be detectable with conventional imaging techniques. It is not inconceivable that the discrepancies in *D* values and bimodal distribution of isovalent cations, reported in some of the previous studies, result from disequilibrium partitioning. For example, decoupling of light and heavy REE in $MgSiO_3$, noted by Hirose *et al.* (2004), can be more plausibly explained by growth-controlled partitioning of larger $LREE^{3+}$ cations into the {100} sectors (see above), rather than by assuming the existence of two different *A* sites in the structure (ibid., p. 255–256). It is intriguing to speculate that in high-pressure silicate perovskites, trivalent cations (Fe^{3+} and Al^{3+}) should favor the {100} sectors (in a cubic setting), whereas Mg^{2+} and Ni^{2+} should be enriched in the {111} sectors relative to Fe^{2+}, Mn^{2+} and Ca^{2+}.

Fast crystallization rates (on the order of 10^{-7} to 10^{-9} m/s for individual faces) employed in experimental studies are conducive to the development of sector zoning, as seen, for example, in clinopyroxene (Kouchi *et al.*, 1983; Skulski *et al.*, 1994). The impeding effect of high pressure on lattice diffusion (*e.g.*, Van Orman *et al.*, 2001) is likely to preserve compositional heterogeneities arising from growth-controlled element partitioning (Watson & Liang, 1995). Interestingly, sector-controlled distribution of trace elements is a "hallmark" of diamonds synthesized at high *P* and *T* (*e.g.*, Shigley *et al.*, 2004), but is relatively uncommon in natural crystals.

Conclusions and future work

The rasvumite and PGrM from Mont Saint-Hilaire hold important clues to the evolutionary history of their host rock (tawite). The enrichment of rasvumite in Rb and Cs, low Ta/Nb ratio in loparite and lueshite, and the association of these minerals with sodalite and villiaumite indicate that this rock crystallized from highly-fractionated peralkaline magma enriched in Cl, F and S. It remains to be determined whether the tawites and their host nepheline syenites are cognate, as proposed by Piilonen *et al.* (1998). The immiscibility model agrees with the available experimental data and petrogenetic interpretation of nepheline-syenite + tawite associations at other localities (Kogarko *et al.*, 1974; Romanchev & Kuznetsova, 1982; Gerasimovskii *et al.*, 1968a), but identification of immiscibility in either synthetic or natural systems is not trivial, and further studies of sodalite crystallization from peralkaline melts are clearly required.

The crystal-chemical analysis of element distribution in the loparite-lueshite intergrowths from MSH and comparison with the published data were used to develop a genetic model for sector zoning in perovskites (*sensu lato*). In this model, the inter-sectorial distribution of elements is controlled by: (i) the differences in bonding geometry of cation protosites exposed on the {100} and {111} surfaces of a growing crystal; (ii) relative bond strength; (iii) charge constraints imposed by heterovalent substitutions within the same sector; and (iv) the chemistry of crystallization environment. The differences in partitioning behavior between high- and low-charged cations are in accord with the general model of Dowty (1976), whereas the partitioning of isovalent *A*-site cations does not agree with Dowty's predictions, but can be readily explained in terms of the differences in bond strength between large and small cations. The distribution of *B*-site cations appears to be controlled primarily by the charge constraints imposed by

substitutions in the *A* site. Finally, inconsistencies in partitioning behavior of Na and Ti among the different PGrM are actually *consistent* with the availability (or otherwise) of certain trace elements (primarily, Nb and LREE) in the crystallization environment. The latter mechanism is not obvious unless a range of perovskite compositions from different rock types is examined. Such comparison shows that the trace-element budget of a melt or fluid may have significant influence on the partitioning of major elements (*e.g.*, Na) between the crystal and melt (fluid).

Although the present work summarizes the data on sector zoning in a wide range of perovskite compositions, we were limited to a small set of analytical data. It is essential to extend this dataset to a larger selection of trace elements and to PGrM from other localities. It is also important to test the applicability of our model to compositions that fall outside the $Na_{0.5}Ce_{0.5}TiO_3$–$NaNbO_3$–$CaTiO_3$–$SrTiO_3$ system. For example, all sector-zoned PGrM described to date contain low levels of trivalent *B*-site cations ($\leqslant$0.5 wt.% Fe, undetectable Al, Cr and V), which can be incorporated in perovskite via two principal substitutions, $Ca^{2+} + Ti^{4+} \Leftrightarrow LREE^{3+} + {}^{[6]}B^{3+}$ and $2Ti^{4+} \Leftrightarrow {}^{[6]}B^{3+} + Nb^{5+}$ (Kopylova *et al.*, 1997; Chakhmouradian & Mitchell, 2001). By analogy with Na, we can expect that Nb-enriched {111} sectors will compete for ${}^{[6]}B^{3+}$ with the LREE-enriched {100} sectors, and that the inter-sectorial partitioning of ${}^{[6]}B^{3+}$ will be controlled predominantly by the availability of LREE and Nb in the melt. Clearly, empirical data are needed to test this conjecture.

Another potential avenue of further research is to study the influence of anion substitutions on sector zoning. The relative importance of charge and size constraints may be different for zoning involving only heterovalent substitutions of cations vs. cases where such exchange is charge-balanced by anion substitutions in the nearest coordination sphere, *e.g.*, $(Al,Fe)^{3+} + O^{2-} \Leftrightarrow Mg^{2+} + (OH)^{1-}$ in tourmaline (Henry *et al.*, 1999). Although it is reasonable to expect that size considerations become more important where alternative charge-compensation mechanisms (*i.e.* anion exchange) are available, this aspect of the crystal chemistry of minerals has not been addressed in the previous literature. An in-depth study of sector-zoned minerals with "mixed" anion populations is required to further our understanding of these mechanisms and their influence on the inter-sectorial distribution of cations.

In conclusion, we would like to add that sector zoning in minerals is a function with many parameters, and, despite the voluminous literature on this subject, some of these parameters remain poorly understood and, possibly, unrecognized.

Acknowledgements: This work was supported by the Natural Sciences and Engineering Research Council of Canada (NSERC). The instrumentation used in the present work was acquired with support from NSERC and Canada Foundation for Innovation. Gilles Haineault is thanked for providing us with the loparite-bearing material, and Anne Hammond for her skilled help with thin-section preparation. The assistance of Ron Chapman, Allan MacKenzie, Panseok Yang and Keith Pringnitz with data acquisition is most gratefully acknowledged. An anonymous reviewer and Editor Ekkehart Tillmanns are cordially thanked for their constructive comments on the earlier version of this paper.

References

Akizuki, M. (1981): Origin of optical variation in analcime. *Am. Mineral.*, **66**, 403-409.

— (1984): Origin of optical variations in grossular-andradite garnet. *Am. Mineral.*, **69**, 328-338.

Brophy, J.G., Wittington, C.S., Park, Y.-R. (1999): Sector-zoned augite megacrysts in the Aleutian high alumina basalts: implications for the conditions of basalt crystallization and the generation of calc-alkaline series magmas. *Contrib. Mineral. Petrol.*, **135**, 277-290.

Brown, I.D. (1996): *VALENCE*: a program for calculating bond valences. *J. Appl. Crystallogr.*, **29**, 479-480.

Bussen, I.V., & Sakharov, A.S. (1972): Petrology of the Lovozero alkaline massif. Nauka, Leningrad, 296 p. (in Russ.).

Černý, P. (1982): Mineralogy of rubidium and cesium. *MAC Short Course Handb.* **8**, 149-161.

Černý, P., Chapman, R., Teerstra, D.K., Novák, M. (2003): Rubidium- and cesium-dominant micas in granitic pegmatites. *Am. Mineral.*, **88**, 1832-1835.

Chakhmouradian, A.R. (2006): High-field-strength elements in carbonatitic rocks: Geochemistry, crystal chemistry and significance for constraining the sources of carbonatites. *Chem. Geol.*, **235**, 138-160.

Chakhmouradian, A.R., & Mitchell, R.H. (1997): Compositional variation of perovskite-group minerals from the carbonatite complexes of the Kola Alkaline Province, Russia. *Can. Mineral.*, **35**, 1293-1310.

—, — (2001): Three compositional varieties of perovskite from kimberlites of the Lac de Gras field (Northwest Territories, Canada). *Mineral. Mag.*, **65**, 133-148.

—, — (2002a): New data on pyrochlore- and perovskite-group minerals from the Lovozero alkaline complex, Russia. *Eur. J. Mineral.*, **14**, 821-836.

—, — (2002b): The mineralogy of Ba- and Zr-rich alkaline pegmatites from Gordon Butte, Crazy Mountains (Montana, USA): comparisons between potassic and sodic agpaitic pegmatites. *Contrib. Mineral. Petrol.*, **143**, 93-114.

Chakhmouradian, A.R., & Mitchell, R.H. Pankov, A.V., Chukanov, N.V. (1999): Loparite and 'metaloparite' from the Burpala alkaline complex, Baikal Alkaline Province (Russia). *Mineral. Mag.*, **63**, 519-534.

Chen, T.T., & Szymañski, J.T. (1982): A comparison of galkhaite from Nevada and from the type locality, Khaydarkan, Kirgizia, U.S.S.R. *Can. Mineral.*, **20**, 575-577.

Czamanske, G.K., Erd, R.C., Sokolova, M.N., Dobrovol'skaya, M.G., Dmitrieva, M.K. (1979): New data on rasvumite and djerfisherite. *Am. Mineral.*, **64**, 776-778.

Cressey, G., Wall, F., Cressey, B.A. (1999): Differential *REE* uptake by sector growth of monazite. *Mineral. Mag.*, **63**, 813-828.

Dawson, J.B., & Hill, P.G. (1998): Mineral chemistry of a peralkaline combeite-lamprophyllite nephelinite from Oldoinyo Lengai, Tanzania. *Mineral. Mag.*, **62**, 179-196.

DeMark, R.S. (1984): Minerals of Point of Rocks, New Mexico. *Mineral. Rec.*, **15(3)**, 149-156.

Dobosi, G., Schultz-Güttler, R., Kurat, G., Kracher, A. (1991): Pyroxene chemistry and evolution of alkali basaltic rocks from Burgenland and Styria, Austria. *Mineral. Petrol.*, **43**, 275-292.

Dowty, E. (1976): Crystal structure and crystal growth: II. Sector zoning in minerals. *Am. Mineral.*, **61**, 460-469.

Gamble, J.A. (1984): Petrology and geochemistry of differentiated teschenite intrusions from the Hunter Valley, New South Wales, Australia. *Contrib. Mineral. Petrol.*, **88**, 173-187.

Gebhard, G., & Schlüter, J. (1994): St. Hilaire, Kanada: Die ersten Kristalle! *Lapis*, **1994(10)**, 34-35.

Gerasimovsky, V.K., Volkov, V.P., Kogarko, L.N., Polyakov, A.I., Saprykina, T.V., Balashov, Yu.A. (1968a): The geochemistry of the Lovozero alkaline massif. Part one: geology and petrology. Austral. Nat. Univ. Press, Canberra.

—, —, —, —, —, —, — (1968b): The geochemistry of the Lovozero alkaline massif. Part two: geochemistry. Austral. Nat. Univ. Press, Canberra.

Grossman, L. (1972): Condensation in the primitive solar nebula. *Geochim. Cosmochim. Acta*, **36**, 597-619.

— (1980): Refractory inclusions in the Allende meteorite. *Ann. Rev. Earth Planet. Sci.*, **8**, 559-608.

Haggerty, S.E. (1987): Metasomatic mineral titanates in upper mantle xenoliths. *in* "Mantle xenoliths", P.H. Nixon, (ed.), Wiley, Chichester, 671-690.

Hartman, P. (1973): Structure and morphology. *in* "Crystal growth: an introduction", P. Hartman, (ed.), North Holland Publ. Co., Amsterdam, 367-402.

Henry, D.J., Kirkland, B.L., Kirkland, D.W. (1999): Sector-zoned tourmaline from the cap rock of a salt dome. *Eur. J. Mineral.*, **11**, 263-280.

Hirose, K., Shimizu, N., Westrenen, W.V., Fei, Y. (2004): Trace element partitioning in earth's lower mantle and implications for geochemical consequences of partial melting at the core-mantle boundary. *Phys. Earth Planet. Int.*, **6**, 249-260.

Holland, T.J.B., & Redfern, S.A.T. (1997): Unit cell refinement from powder diffraction data: the use of regression diagnostics. *Mineral. Mag.*, **61**, 65-77.

Horváth, L., & Gault, R.A. (1990): The mineralogy of Mont Saint-Hilaire, Québec. *Mineral. Rec.*, **21**, 284-368.

Horváth, L., & Pfenninger-Horváth, E. (2000): I minerali di Mont Saint-Hilaire. *Rivista Mineral. Ital.*, **24**, 140-202.

Hu, M., Wenk, H.-R., Sinitsyna, D. (1992): Microstructures in natural perovskites. *Am. Mineral.*, **77**, 359-373.

Ifantopulo, T.N., Yushko-Zakharova, O.E., Dubakina, L.S., Shcherbachev, D.K. (1983): Rasvumite from the Lovozero massif. *Doklady Akad. Nauk SSSR*, **269**, 195-197 (in Russ.).

Jago, B.C., & Gittins, J. (1999): Mn- and F-bearing rasvumite in natrocarbonatite at Oldoinyo Lengai volcano, Tanzania. *Mineral. Mag.*, **63**, 53-55.

Jamtveit, B., Dahlgren, S., Austrheim, H. (1997): High-grade contact metamorphism of calcareous rocks from the Oslo Rift, Southern Norway. *Am. Mineral.*, **82**, 1241-1254.

Jensen, B.B. (2000): Partitioning of elements in sector-zoned clinopyroxenes. *Mineral. Mag.*, **64**, 725-728.

Kogarko, L.N., Ryabchikov, I.D., Sørensen, H. (1974): Liquid fractionation. *in* "The alkaline rocks", H. Sørensen, ed., John Wiley & Sons, London, 488-500.

Kopylova, M.G., Rickard, R.S., Kleyenstueber, A., Taylor, W.R., Gurney, J.J., Daniels, L.R.M. (1997): First occurrence of strontian K-Cr loparite and Cr-chevkinite in diamonds. *Russ. Geol. Geophys.*, **38**, 405-420.

Kouchi, A., Sugawara, Y., Kashima, K., Sunagawa, I. (1983): Laboratory growth of sector zoned clinopyroxenes in the system $CaMgSi_2O_6$-$CaTiAl_2O_6$. *Contrib. Mineral. Petrol.*, **83**, 177-184.

Le Maitre, R.W., ed. (2002): Igneous rocks: a classification and glossary of terms. Cambridge Univ. Press, Cambridge, 236 p.

Lloyd, F.E., Edgar, A.D., Ragnarsdottir, K.V. (1996): LREE distribution in perovskite, apatite and titanite from South West Ugandan xenoliths and kamafugite lavas. *Mineral. Petrol.*, **57**, 205-228.

McDonald, A.M., & Chao, G.Y. (2004): Haineaultite, a new hydrated sodium calcium titanosilicate from Mont Saint-Hilaire, Quebec: description, structure determination and genetic implications. *Can. Mineral.*, **42**, 769-780.

McDonough, W.F., & Sun, S.-s. (1995): The composition of the Earth. *Chem. Geol.*, **120**, 223-253.

Mitchell, R.H., Burns, P.C., Chakhmouradian, A.R. (2000): The crystal structures of loparite-(Ce). *Can. Mineral.*, **38**, 145-152.

Mitchell, R.H., Ross, K.C., Potter, E.G. (2004): Crystal structures of $RbFe_2S_3$ and $CsFe_2S_3$: synthetic analogs of rasvumite KFe_2S_3. *J. Solid State Chem.*, **177**, 1867-1872.

Mitchell, R.H., & Chakhmouradian, A.R. (1996): Compositional variation of loparite from the Lovozero alkaline complex, Russia. *Can. Mineral.*, **34**, 977-990.

—, — (1999): Sr-bearing perovskite and loparite from lamproite and agpaitic nepheline syenite pegmatites. *Can. Mineral.*, **37**, 99-112.

Noguera, C. (2000): Polar oxide surfaces. *J. Phys. Cond. Mat.*, **12**, R367-R410.

Paquette, J., & Reeder, R.J. (1995): Relationship between surface structure, growth mechanism, and trace element incorporation in calcite. *Geochim. Comsochim. Acta*, **59**, 735-749.

Paterson, B.A., & Stephens, W.E. (1992): Kinetically induced compositional zoning in titanite: implications for accessory-phase/melt partitioning of trace elements. *Contrib. Mineral. Petrol.*, **109**, 373-385.

Pearce, N.J.G., Perkins, W.T., Westgate, J.A., Gorton, M.P., Jackson, S.E., Neal, C.R., Chenery, S.P. (1997): A compilation of new and published major and trace element data for NIST SRM 610 and NIST SRB 612 glass reference materials. *Geostand. Newslet.*, **21**, 115-144.

Pekov, I.V., & Podlesnyi, A.S. (2004): Kukisvumchorr deposit: mineralogy of alkaline pegmatites and hydrothermalites. Assoc. Ecost and Ocean Pictures Ltd, Moscow, Russia.

Piilonen, P.C., McDonald, A.M., Lalonde, A.E. (1998): The crystal chemistry of aegirine from Mont Saint-Hilaire, Quebec. *Can. Mineral.*, **36**, 779-791.

Piilonen, P.C., Lalonde, A.E., McDonald, A.M., Gault, R.A., Larsen, A.O. (2003): Insights into astrophyllite-group minerals. I. Nomenclature, composition and development of a standardized general formula. *Can. Mineral.*, **41**, 1-26.

Romanchev, B.P., & Kuznetsova, S.Ya. (1982): The conditions of nosean crystallization in alkaline melts. *Izvest. Akad. Nauk SSSR, Ser. Geol.*, **1982 (1)**, 134-137 (in Russ.).

Searl, A. (1990): Complex sector zonation in ankerite: geochemical controls on crystal morphology and intersector element partitioning. *Mineral. Mag.*, **54**, 501-507.

Shannon, R.D. (1976): Revised effective ionic radii and systematic studies of interatomic distances in halides and chalcogenides. *Acta Crystallogr.*, **A32**, 751-767.

Shearer, C.K., & Larsen, L.M. (1994): Sector-zoned aegirine from the Ilimaussaq alkaline intrusion, South Greenland: Implications for trace-element behavior in pyroxene. *Am. Mineral.*, **79**, 340-352.

Shigley, J.E., Breeding, C.M., Hsi-Tien Shen, A. (2004): An updated chart on the characteristics of HPHT-grown synthetic diamonds. *Gems Gemol.*, **40**, 303-313.

Simon, S.B., Kuehner, S.M., Davis, A.M., Grossman, L., Johnson, M.L., Burnett, D.S. (1994): Experimental studies of trace element partitioning in Ca,Al-rich compositions: Anorthite and perovskite. *Geochim. Cosmochim. Acta*, **58**, 1507-1523.

Skulski, T., Minarik, W., Watson, E.B. (1994): High-pressure experimental trace-element partitioning between clinopyroxene and basaltic melts. *Chem. Geol.*, **117**, 127-147.

Sokolova, E., Huminicki, D.M.C., Hawthorne, F.C., Agakhanov, A.A., Pautov, L.A., Grew, E.S. (2002): The crystal chemistry of telyushenkoite and leifite, $A Na_6[Be_2Al_3Si_5O_{39}F_2]$, A = Cs, Na. *Can. Mineral.*, **40**, 183-192.

Sokolova, M.N., Dobrovol'skaya, M.G., Organova, N.I., Kazakova, M.E., Dmitrik, A.L. (1970): Sulfide of potassium and iron – the new mineral rasvumite. *Zapiski Vses. Mineral. Obshchest.*, **99**, 712-720 (in Russ.).

Taura, H., Yurimoto, H., Kato, T., Sueno, S. (2001): Trace element partitioning between silicate perovskites and ultracalcic melt. *Phys. Earth Planet. Int.*, **124**, 25-32.

van Achterbergh, E., Ryan, C.G., Griffin, W.L. (2001): GLITTER on-line interactive data reduction for the LA-ICPMS microprobe. Macquarie Research Ltd., Sydney.

Van Orman, J.A., Grove, T.L., Shimizu, N. (2001): Rare earth element diffusion in diopside: influence of temperature, pressure, and ionic radius, and an elastic model for diffusion in silicates. *Contrib. Mineral. Petrol.*, **141**, 687-703.

Vorob'yov, E.I., Konev, A.A., Malyshonok, Yu.V., Afonina, G.G., Paradina, L.F. (1987): Tausonite: geological formation conditions and mineral parageneses. Nauka, Novosibirsk (in Russ.).

Wang, S.C., & Ehrlich, G. (1991): Atom incorporation at surface clusters: An atomic view. *Phys. Rev. Lett.*, **67**, 2509-2512.

Wass, S.Y. (1973): Origin and petrogenetic significance of hourglass zoning in titaniferous clinopyroxenes. *Mineral. Mag.*, **39**, 133-144.

Watson, E.B., & Liang, Y. (1995): A simple model for sector zoning in slowly grown crystals: Implications for growth rate and lattice diffusion, with emphasis on accessory minerals in crustal rocks. *Am. Mineral.*, **80**, 1179-1187.

Wight, Q., & Chao, G.Y. (1995) Mont Saint-Hilaire revisited, Part 2. *Rocks Minerals*, **70**, 90-103, 131-138.

Wood, B.J. (2000): Phase transformations and partitioning relations in peridotite under lower mantle conditions. *Earth Planet. Sci. Lett.*, **174**, 341-354.

Woolley, A.R., & Platt, R.G. (1988): The peralkaline nepheline syenites of the Junguni intrusion, Chilwa Province, Malawi. *Mineral. Mag.*, **52**, 425-433.

Yudintsev, S.V., Xuan, Ph.T., Gramenetskiy, Ye.N., Shchekina, T.I. (1983): Experimental modeling of formation of nepheline syenite pegmatite. *Doklady Earth Sci. Sect.*, **268**, 119-122.

Received 9 February 2006
Modified version received 8 March 2007
Accepted 7 Mai 2007